

Detecting Compton Reflection and a Broad Iron Line in MCG–5-23-16 with *RXTE*

K. A. Weaver

Johns Hopkins University, Department of Physics and Astronomy, Homewood Campus,
3400 North Charles Street, Baltimore, MD 21218-2695; e-mail: kweaver@pha.jhu.edu

and

J. H. Krolik

Johns Hopkins University, Department of Physics and Astronomy, Homewood Campus,
3400 North Charles Street, Baltimore, MD 21218-2695

and

E. A. Pier

NASA Goddard Space Flight Center, Laboratory for High Energy Astrophysics, Greenbelt,
MD 20771

ABSTRACT

We report the detection with the Rossi X-ray Timing Explorer of a Compton reflection signature in the Seyfert galaxy MCG–5-23-16. *RXTE* also resolves the Fe $K\alpha$ fluorescence line with FWHM $\sim 48,000$ km s $^{-1}$. This measurement provides the first *independent* confirmation of *ASCA* detections in Seyfert galaxies of broad Fe $K\alpha$ lines that are thought to be the signature of emission from the inner regions of an accretion disk orbiting a black hole. Under the assumption that reflection arises from an isotropic source located above a neutral accretion disk, and using a theoretical model that accounts for the dependence of the reflected spectrum on inclination angle, we derive a 90% confidence range for the disk inclination of $i = 50^\circ - 81^\circ$. The large inclination is consistent with that expected from the unified model for MCG–5-23-16 based on its Seyfert 1.9 classification. If we assume that the high-energy cutoff in the incident spectrum lies at energies larger than a few hundred keV, then the equivalent width of the Fe $K\alpha$ line is much larger than predicted for the amount of reflection. This implies either an enhanced iron abundance, a covering factor of reflecting material $c_f > 0.5$, or a cutoff in the incident spectrum at energies between ~ 60 and ~ 200 keV.

Subject headings: galaxies: individual (MCG-5-23-16) - galaxies: nuclei -
galaxies: Seyfert - X-rays: galaxies

1. Introduction

At the heart of an active galactic nucleus lies the putative black-hole “monster” that supplies its power. Much of this power emerges in the form of X-rays, which are in turn efficient probes of the immediate regions surrounding the nucleus. The fuel supply for the massive central engine is thought to arise from a disk of dense, accreting matter with column densities N_{H} well in excess of $\sim 10^{24} \text{ cm}^{-2}$. In the presence of such matter, the reflected X-ray spectrum has two distinct features. One is the Fe $K\alpha$ fluorescence emission line at 6.4 keV (Fabian et al. 1989, George & Fabian 1991). The other is Compton reflection, a broad hump centered on a few tens of keV with a shape governed by photoelectric absorption at low energies and by Compton recoil and the declining scattering cross-section at high energies (Lightman & White 1988; Guilbert & Rees 1988).

The ubiquity of Fe $K\alpha$ lines in Seyfert galaxies is well established. Recent results from the Advanced Satellite for Cosmology and Astrophysics (*ASCA*) suggest that many of these lines in Seyfert 1 galaxies exhibit relativistic profiles that are caused by photons emerging near a black hole, and thus they most likely originate in an accretion disk (Nandra et al. 1997). Whether Compton reflection is as common is not known. Although hard X-ray observations with *Ginga* show that Compton reflection is clearly present in the *composite* spectrum of eight bright Seyfert 1 galaxies (Pounds et al. 1990), the level of significance of this feature and constraints for theoretical reflection models are poor for most *individual* objects in the *Ginga* sample (Smith & Done 1996, Nandra & Pounds 1994). The Rossi X-ray Timing Explorer (*RXTE*) provides the large bandpass coverage and collecting area necessary to allow the unambiguous detection of Compton reflection in many individual Seyfert galaxies for the first time.

MCG–5-23-16 is an X-ray bright active galaxy with an optical classification of Seyfert 1.9 (Veron et al. 1980). In the 20 years since its discovery, its 2 to 10 keV flux has varied by a factor of 4 from a high state of $\sim 8 \times 10^{-11} \text{ ergs cm}^{-2} \text{ s}^{-1}$ in 1978 (Tennant 1983), to a low state of $\sim 2 \times 10^{-11} \text{ ergs cm}^{-2} \text{ s}^{-1}$ in 1989 (Nandra & Pounds 1994), to a high state of $\sim 9 \times 10^{-11} \text{ ergs cm}^{-2} \text{ s}^{-1}$ in 1996 (this work). In its high-flux state, MCG–5-23-16 is among the five brightest Seyfert galaxies in hard X-rays. *ASCA* observations show the Fe $K\alpha$ line to be significantly broadened with a FWZI of $\sim 120,000 \text{ km s}^{-1}$ and an unusually complex profile (Weaver et al. 1997, hereafter W97). The signature of Compton reflection has not before been detected in this galaxy.

Here we present the first results for MCG–5-23-16 from *RXTE*. This work showcases the data quality, and more importantly, the power of using *RXTE* for purposes of X-ray spectroscopy studies of active galaxies. This paper describes early results from a comprehensive spectral and variability study of MCG–5-23-16 that involves simultaneous

ASCA observations. The *ASCA* results and a joint analysis of the *ASCA* and *RXTE* data will be presented in a future paper.

2. Observations and Data Selection

RXTE was launched on 30 December 1995 and carries three scientific instruments: the Proportional Counter Array (PCA), the High-Energy X-ray Timing Experiment (HEXTE), and the All-Sky Monitor (ASM). Here we present data from the PCA, which consists of five collimated (1° FWHM) proportional counter units (PCUs) that contain three multi-anode detector layers with a mixture of xenon and methane gas. The PCUs are numbered 0 through 4. Each has a bandpass of 2 to 60 keV, a geometric collecting area of $\sim 1,400$ cm², and a FWHM energy resolution of $\sim 8\%$ at 6.6 keV. See Glasser, Odell, and Seufert (1994) for a detailed description of the PCA.

MCG–5-23-16 was observed with *RXTE* from November 27 to 30 1996, for about ~ 100 ks. There was an overlapping observation with *ASCA* that began about half way through the *RXTE* observation on 29 November 1996 and lasted for approximately 35 ks. We do not discuss the most recent *ASCA* data here except to use the observed photon index and absorbing column density (Weaver et al., in prep) to constrain the *RXTE* fits.

To maximize the signal-to-noise ratio between 2 and 10 keV, we accumulate photon events from the top xenon/methane layer of the PCA. We also use only PCUs 0 through 3; data from PCU 4 is discarded because this detector is turned on for a smaller fraction of the on-source time due to breakdown. Data is discarded for times of Earth occult (when the Earth elevation angle is less than 10°), passage of the satellite through the South Atlantic Anomaly (SAA), and when there is severe electron contamination. This yields a total integration time of ~ 80 ksec. For the total spectrum, the small statistical errors on the data points combined with systematic uncertainties in the detector response matrix cause large values of χ^2 . Also, the background subtraction is not yet accurate for the complete observation due to small variations in the internal background that are not accounted for in the current background model. We therefore use an 11 ksec exposure that coincides with the *ASCA* observation on 29 November 1996, and is accumulated from 9.188×10^7 s to 9.191×10^7 s *RXTE* mission elapsed time. For this snapshot, Poisson statistics are an acceptable description of the point to point variations in the data, the systematic errors have a minimal impact on our results because they are comparable to the statistical errors, and the background model works appropriately.

The PCA detector response matrix was generated by adding together matrices for

PCUs 0, 1, 2, and 3 that were supplied by the *RXTE* Guest Observer Facility (GOF) at the Goddard Space Flight Center. The individual matrices represent the most up-to-date PCA calibration and were created 26 August 1997 using *pcarmf* v2.2.1. At the time of this writing the in-flight energy resolution of the PCA detectors has not been precisely determined, but based on spectral fits to line emission from Cas-A, the most likely value has been measured to within $\sim 1\%$ (Keith Jahoda, 1997 private communication). We therefore use two response matrices that bracket the possible values of the energy resolution. The v2.2.1 matrix has a FWHM resolution of 7.5% at 6.6 keV (resolution factor of 0.75) as the default value. The two response matrices that bracket the most appropriate value for Cas-A have multiplicative factors of 1.07 and 1.13 on the default resolution yielding effective resolution factors of 0.8 and 0.85, or 8.0% and 8.5% FWHM resolution at 6.6 keV. These response matrices are labeled M8 and M85 in the spectral fits discussed below. In the work presented here, the uncertainty in the resolution only affects the significance of detection of the broad Fe $K\alpha$ line. Power-law fits to the spectrum of the Crab with the v2.2.1 response matrix yield residuals less than 2% at all energies included in our fits (Keith Jahoda, 1997 private communication).

The amount of background internal to the PCUs varies according to the orbital environment of the satellite. There are no detectors offset from the science axis to allow a simultaneous measurement of the background, and so the standard procedure that has been developed by the *RXTE* GOF is to model the internal and cosmic background. The background for MCG–5-23-16 was modeled in February 1997 with the *pcabackest* program. The internal background was predicted from the particle and activation models that have been derived from Earth-occult data. The particle model is based on the value of the housekeeping parameter Q6, which tracks the instantaneous particle flux by measuring the rate of events that trigger exactly 6 of the lower level discriminators in each PCU. The activation model estimates the additional background that is present in the detectors after the satellite passes through an SAA.

After background subtraction, the PCA count rate for MCG–5-23-16 is ~ 40 counts s^{-1} . The 11 ksec spectrum contains $\sim 4.4 \times 10^5$ photons. We estimate that the current background model is reliable up to energies of 30 keV and ignore pulse-height channels above this energy. Channels below 2.8 keV are ignored because of remaining calibration uncertainties involving partial charge collection (Keith Jahoda, 1997 private communication). Data are modeled with the *XSPEC* spectral fitting package and χ^2 statistics are used.

3. Spectroscopic Results

MCG–5-23-16 has a large absorbing column of $N_{\text{H}} \sim 2 \times 10^{22} \text{ cm}^{-2}$. This column is measurable with the PCA, but because of ongoing calibration issues at the lowest energies, a systematic error may exist in this measurement that would affect our spectral results. Therefore, we use the information that the simultaneous *ASCA* data provide near energies of 2 keV to place an additional constraint on our spectral modeling. In all cases, we fix the absorbing column density at $N_{\text{H}} = 1.65 \times 10^{22} \text{ cm}^{-2}$ (Weaver et al., in prep), which was obtained by fitting the most recent (simultaneous with *RXTE*) *ASCA* data from 1 – 4.5 keV with an absorbed power-law model. This column is identical to that measured during the 1994 observation ($N_{\text{H}} = 1.62 \pm 0.2 \times 10^{22} \text{ cm}^{-2}$; W97).

The results of spectral fitting are listed in Table 1. We use three models to describe the spectrum: a power law ($N_{\text{E}} \propto E^{-\Gamma}$), a power law plus a Gaussian, and a Compton reflection model plus a Gaussian. The reflection model is the *pexrav* model in *XSPEC*, which is an exponentially cut-off power-law spectrum reflected from a disk of neutral material (Magdziarz & Zdziarski 1995). The free parameters are the photon index of the primary power-law spectrum (Γ), the cutoff energy of the primary power-law spectrum (E_c), the abundance of heavy elements (Z), the relative amount of reflection compared to the directly-viewed primary spectrum (R), the inclination angle of the disk normal to our line of sight (i), and the power-law normalization (A). The quantity R is equal to 1 for the case of an isotropic X-ray source above a disk with a covering factor $c_f = 0.5$ ($\Omega = 2\pi$) as viewed from the X-ray source.

The amount of reflected flux depends on i and Z , with larger inclinations and/or larger abundances producing less reflection (George & Fabian 1991). In addition, because of the contribution to the reflection hump by down-scattering of high energy photons, the amount of reflection depends on the cutoff energy of the primary power-law spectrum. If E_c is larger than a few hundred keV, there is no significant reduction in the amount of reflection at <30 keV in comparison to a pure power-law spectrum; however, if E_c is less than a few hundred keV, there are fewer primary photons that can scatter to energies below 30 keV. To test the effect of varying E_c , we examine models with $E_c = 60$ keV, 200 keV, and 500 keV. Cutoff energies much less than 60 keV are unlikely because they provide poor fits unless $\Gamma < 1.75$, which is outside the range of indices allowed for the intrinsic spectrum by the simultaneous *ASCA* data (Weaver et al., in prep). A value of $E_c = 200$ keV approximates the cutoff implied by fits to non-simultaneous OSSE and *Ginga* data for MCG–5-23-16 (Fig. 7 in Zdziarski, Johnson, & Magdziarz 1996) and is similar to the mean cutoff energy for radio-quiet Seyfert 1 galaxies (Gondek et al. 1996). The upper limit of 500 keV is chosen simply to have no appreciable effect in the PCA bandpass. We also assume

Solar abundances and allow only one of the parameters R and i to be free for a given fit.

For all models, the spectral parameters and statistical error bars that are derived using response matrices M8 and M85 (§2) are similar, if not identical, and so we list only the numbers derived using M8 in the table (columns 2 through 8). The difference between M8 and M85 does matter when assessing the significance of detection of the broad Fe K α line. We therefore list the values of χ^2/ν , the F-statistic, and the probability of exceeding F for both M8 and M85 in columns 10, 11, and 13 – 16. For fits that include reflection, we also list three best-fit values for the parameters that are most dependent on E_c . These are the iron line equivalent width ($W_{\text{K}\alpha}$, column 5) and i or R (columns 7 and 8). The top entry corresponds to $E_c = 500$ keV, the middle entry corresponds to $E_c = 200$ keV, and the bottom entry corresponds to $E_c = 60$ keV.

Models that do not include reflection provide formally unacceptable fits. An absorbed power law with E_c placed above the PCA bandpass provides an extremely poor fit (Table 1, fit 1) with $\chi^2/\nu > 9$ for 57 d.o.f. The poorness of this fit is illustrated in Figure 1, which shows the PCA data and the power-law model folded through the instrumental response. The residuals for the fit are plotted in the bottom panel. Adding a narrow Gaussian to the model provides a large improvement (Table 1, fit 2, Fig. 2a), but the fit is still statistically unacceptable with $\chi^2/\nu \sim 1.5$ for 55 d.o.f. The probability of obtaining such a large value of χ^2 by chance is only ~ 0.01 . If the line is allowed to be broad (Table 1, fit 3, Fig. 2b), the fit is improved significantly for response M8, but not for M85, as indicated by the small F-statistic and large probability of exceeding F in columns 14 and 16. This fit, however, remains formally unacceptable for both matrices (columns 10 and 11) with a probability of ~ 0.02 for obtaining such large values of χ^2 by chance.

Models that include reflection provide formally acceptable fits (Table 1, fits 4 – 7). To examine how significant this improvement is compared to models that include only the iron line, we compare the fit with a power law and a broad Gaussian (fit 3), to a fit with a power law plus reflection and a narrow Gaussian (fit 4, Fig. 2c). For the fit with reflection, the decrease in χ^2 is large compared to the fit without reflection; $\Delta\chi^2 = 14$ for M8 and $\Delta\chi^2 = 21$ for M85. F-statistic values are not listed for fit 4 because the F-statistic cannot be used in this case to accept or reject the hypothesis that reflection provides a better fit to the data than a broad line. Instead, we calculate the ratio of likelihoods (Edwards 1972) for the reflection plus narrow Gaussian model versus the power law plus broad Gaussian model. This ratio is defined as $L_1/L_2 = \exp[\Delta\chi^2/2]$ for two models. We find that reflection plus a narrow Gaussian is 1,100 to 36,000 times more likely to be the correct description of the data than a power law and broad Gaussian, assuming that the errors are normally distributed.

We next examine whether a broad line is detected when reflection is included in the model (Table 1, fits 5 to 7). To test the range of allowed parameter space, we assume different values for i and R . For fits 5 and 6, we fix i at values of 50° and 87° , which cover the range of most likely inclinations for a neutral accretion disk measured from *ASCA* studies of the Fe $K\alpha$ line profile (W97). Angles less than 50° are the least preferred by the *RXTE* data because they yield poor fits unless E_c is as low as $\sim 30 - 50$ keV, which we have already ruled out since this requires the intrinsic spectrum to be too flat. For $i = 50^\circ$, R is small and ranges from 0.36 to 0.80 implying covering factors of $c_f = 0.18 - 0.40$; however, for $i = 87^\circ$, R is large and ranges from 2.9 to 5.9, implying unphysical covering factors of $c_f > 1.0$. If we instead fix R at 1.0 (fit 7), then i ranges from 63° to 81° (best-fit values) with a 90% confidence range of 50° to 87° . Our results clearly show that R , i , and E_c are strongly coupled. For a given R , smaller inclinations and $W_{K\alpha}$ are allowed for a low E_c , while for a given i , a low E_c allows more reflection and hence a larger c_f . The confidence contours for fit 7 for the width of the Fe $K\alpha$ line vs. i for $E_c = 200$ keV are shown in Figure 3. For all of the above cases, a broad line significantly improves the fit over a narrow line, as indicated by the F-statistic > 3.8 . The probability of exceeding F by chance ranges from 0.05 for the worst case (and the poorest overall fit) to < 0.001 . For fit 7, the $2 - 10$ keV flux is $\sim 9.5 \times 10^{-11}$ ergs cm^{-2} s^{-1} .

Finally, we examine whether the gas that reprocesses X-rays is ionized by replacing the *pegrav* model, which calculates reflection from a neutral disk, with the *pexriv* model, which calculates reflection from an ionized disk. The *pexriv* model adds the free parameters of disk temperature and ionization parameter, but yields no improvement to the fit compared to the neutral case. Also, the best-fitting ionization parameter is zero. This result is consistent with the fact that the peak energy of the Fe $K\alpha$ line is approximately equal to that expected for fluorescence from neutral iron (6.4 keV in the galaxy rest frame), and rules out significant ionization of the disk.

We conclude that Compton reflection *and* a broad Fe $K\alpha$ line from a dense, neutral reflector are detected in MCG–5-23-16 with *RXTE*. In an 11 ksec exposure, the line width is well constrained. There is also little difficulty in statistically separating the reflection component from the broad iron line, a problem that has plagued the analysis of data from missions such as *ASCA* and *Ginga*.

4. Discussion

We have shown that both Compton reflection and a broad Fe $K\alpha$ line are detected in the *RXTE* spectrum of MCG–5-23-16. This is the first clear detection of reflection in this

galaxy, and the broad Fe $K\alpha$ line confirms the reality of the broad line in the *ASCA* data (W97). Detecting a broad Fe $K\alpha$ line with *RXTE* in a Seyfert 1.9 galaxy provides the first independent confirmation of *ASCA* detections of broad lines in these objects. This also puts to rest the idea that the broad lines seen by *ASCA* are spurious features caused by a “continuum conspiracy”, where a complex continuum mimics a broad line.

The significance of detection of the broad line (i.e., having $\sigma > 0.24$ keV) depends somewhat on the response matrix. However, even for the worst-fitting reflection model, a broad line is detected at $\geq 95\%$ confidence. For the best-fitting reflection models, a broad line is detected at greater than 99% confidence.

Examining the parameter space for reflection models, we tested disk inclinations that range from $i = 50^\circ$ to 87° , as suggested by a detailed study of the Fe $K\alpha$ profile (W97). The parameters of disk inclination (i), the amount of reflection (R), and the high-energy cutoff (E_c) are strongly correlated. If we allow the amount of reflection to be a free parameter, then an angle of 50° provides the poorest fit of the models we tested. For $E_c = 500$ keV, R is small but for $E_c = 60$ keV, R becomes consistent with 1, which is the value expected if the reprocessing gas is in the form of a disk. An angle of 87° provides the best fit, but for this case we find the opposite result: for $E_c = 500$ keV, R is consistent with 1, but for $E_c = 60$ keV, R is quite large and implies an unphysical covering factor of neutral reflecting material of $c_f > 1.0$. Assuming instead a normal disk geometry with $c_f = 0.5$ ($R = 1$), the fit is statistically comparable to the best-fit, and we confirm the above result, namely that i can range from 50° to 87° for high-energy cutoffs in the primary spectrum ranging from 60 to 500 keV.

The model parameters derived from *RXTE* are similar to those derived from *ASCA* (W97). For a reflection model with $c_f = 0.5$, $\Gamma(\textit{ASCA})$ ranges from 1.84 to 2.05 (90% confidence errors) depending on how the Fe K line is modeled, while the mean value for *RXTE* from reflection-model fits is $\Gamma(\textit{RXTE}) = 1.82 \pm 0.10$. The indices are consistent although not necessarily identical, but this is not a problem since the photon index varies in this galaxy (W97). Comparing the Fe K-line parameters is not straightforward because the line is clearly non-Gaussian (W97) and the energy resolutions of the experiments differ by a factor of four. However, the line parameters are consistent for a single-Gaussian approximation. In *ASCA*, the line has $E_{\text{peak}} = 6.37 \pm 0.05$ keV, $W_{K\alpha} \sim 260$ eV, $\sigma \sim 0.5$ keV, and $\text{FWZI} \sim 2.4$ keV (W97). In *RXTE*, the line has $E_{\text{peak}} = 6.26_{-0.11}^{+0.09}$ keV, $W_{K\alpha} = 230_{-22}^{+25}$ eV, $\sigma = 0.43 \pm 0.15$ keV, and $\text{FWZI} \sim 2.5$ keV.

The inclination of the accretion disk is determined by different methods for the two experiments. For *RXTE*, it is measured from the amount of Compton reflection, and for *ASCA*, it is measured from the shape of the Fe $K\alpha$ line. W97 and Turner et al. (1997;

hereafter T97) derive different inclinations from *ASCA* using different techniques. Both authors use a model that consists of a theoretical line profile from an accretion disk (a ‘disk line’; Fabian et al. 1989, Laor 1991) and assume fluorescence from a neutral disk with $c_f = 0.5$; however, W97 use a two-component model that consists of a disk line and a narrow Gaussian at 6.4 keV (which represents emission from gas further out), while T97 fit the entire line with a disk line. Additionally, W97 assume an outer disk radius of $r_o = 400r_g$ ($r_g = GM/c^2$) and derive the following three parameters: the disk emissivity index, q (r^{-q}), the inner disk radius, r_i , and the inclination (i). Using a different approach, T97 assume $r_i = 6r_g$, $r_o = 1000r_g$, and $q = 2.5$ and derive only i . Depending on the choice of Schwarzschild or Kerr geometries, W97 find $q = 5$ to 7 , $r_i = 13$ to $22r_g$, $i = 52^\circ$ to 89° , $W_{K\alpha}(\text{Gaussian}) = 54$ to 69 eV, and $W_{K\alpha}(\text{disk line}) = 198$ to 223 eV. Using a Schwarzschild geometry, T97 find $i = 33_{-4}^{+11}$ ° and $W_{K\alpha}(\text{total}) = 362_{-43}^{+94}$. It is not possible to prove which assumptions are correct because the geometry of the disk, the emissivity profile as a function of radius, and even whether or not all of the fluorescence arises from an accretion disk, are not known *a priori*. We conclude that the inclination derived from the line profile does not necessarily represent of the true inclination of the accretion disk. The range of inclinations derived from *RXTE* from the amount of Compton reflection is $50^\circ - 87^\circ$ (90% confidence), in agreement with W97.

One problem for all of these analyses, including the current one, is the large equivalent width of the disk line. For $E_c = 500$ keV, we find $W_{K\alpha} \sim 230$ eV with *RXTE*, which is much larger than the maximum equivalent width of 160 eV predicted from a neutral disk (George & Fabian 1991). The $W_{K\alpha}$ of the disk line can be reduced if we follow W97 and assume that $\sim 25\%$ of the iron line flux originates from somewhere other than the disk. In this case, we find $W_{K\alpha}(\text{disk line}) \sim 170$ eV. This is still a problem, however, because the equivalent width for an edge-on disk is expected to be much smaller than 160 eV. In fact, $W_{K\alpha}$ predicted for a neutral disk viewed at our best-fitting inclination of 81° for an incident spectrum with $\Gamma = 1.9$ is only ~ 50 eV (George & Fabian 1991). Clearly, there is too much flux in the iron line to be produced by such a disk. Large equivalent widths can be produced if the accretion disk is ionized, but the *RXTE* data rule out this possibility.

Besides the dependence of $W_{K\alpha}$ on disk inclination and Γ , $W_{K\alpha}$ is proportional to the iron abundance and the covering factor of reflecting material. If we assume almost complete coverage of the X-ray source ($c_f = 0.99$), an equivalent width as large as 170 eV restricts the disk to be inclined by no more than 70° (George & Fabian 1991). For the case of $E_c = 500$ keV, this inclination is inconsistent with our statistical lower limit of 73° (Table 1). Thus it is impossible to have a self-consistent interpretation of the data for $E_c = 500$ keV without having a factor of ~ 3 overabundance of iron.

For smaller cutoff energies, smaller inclinations are allowed. For $E_c = 60$ and 200 keV, the 90% confidence range of inclinations is 50° to 81° , which allows equivalent widths as large as ~ 130 eV for a neutral disk with $c_f = 0.5$. To produce a value as large as $W_{K\alpha} = 170$ eV, it is thus possible to have c_f as small as 0.65 and still have solar abundances. If iron is overabundant, c_f can be less. This technique of comparing the relative fluxes in the Fe K line and reflection hump thus allows us to infer the presence of a high-energy cutoff in the intrinsic spectrum and to place approximate limits on E_c of 60 to 200 keV. Our analysis clearly demonstrates the model-dependence of disk inclination angle and covering factor on the shape of the incident spectrum and provides a self-consistent explanation of the data without invoking unusually large abundances.

The unified model describes Seyfert 1 galaxies as having their nuclear regions viewed preferentially at small inclination angles so that the continuum source and broad line region are not blocked. Conversely, this model describes Seyfert 2s and intermediate types (i.e., Seyfert 1.8s and 1.9s) as having their inner regions viewed preferentially edge-on so that the continuum source and broad line region are blocked by thick clouds. Within the context of this model, the mean inclinations for the two types are predicted to be $\sim 30^\circ$ and $\sim 60^\circ$ for 1s and 2s, respectively. Seyfert 1 galaxies appear to follow the expected trend, with a mean inclination angle of 30° (Nandra et al. 1997). On the other hand, Seyfert 2 galaxies may not follow the expected trend. T97 derive small angles of 13 to 33° for four Seyfert 1.9 and 2 galaxies, including MCG–5-23-16, and conclude that these objects have their inner regions preferentially seen face on, similar to Seyfert 1s. In contrast, the *RXTE* data imply that the disk in MCG–5-23-16 is viewed edge-on. The 90% confidence range of inclinations inferred from fits with Compton reflection models, 50° to 81° , is entirely consistent with the geometry of the nuclear region that is predicted by the unified model based on its Seyfert 1.9 classification.

Clearly, *RXTE* provides valuable information that can be used to constrain the geometry and distribution of gas near the centers of active galaxies. Comparing results in the literature, we find that using *ASCA* data alone to derive disk inclinations from iron line profiles is ambiguous because there are many unknown parameters and the results depend crucially on the assumptions that go into the modeling. Although an approximately face-on disk can be derived for certain techniques of modeling the *ASCA* data, this interpretation is not supported by the *RXTE* data, which instead favor large inclinations.

5. Conclusion

Using *RXTE*, we have detected the signature of Compton reflection in the Seyfert 1.9 galaxy MCG–5-23-16. We also confirm the broad Fe K α line seen with *ASCA* with FWHM $\sim 48,000$ km s $^{-1}$. This measurement provides an independent confirmation of the broad line that is thought to be the signature of emission from the inner regions of an accretion disk orbiting a black hole. From spectral modeling, we derive a 90% confidence range for the disk inclination of $50^\circ - 81^\circ$, which is consistent with the inclination predicted from the unified model for MCG–5-23-16 based on its Seyfert 1.9 classification. The equivalent width of the Fe K α line from the disk is at least ~ 170 eV. This is much larger than that predicted for a highly inclined, neutral accretion disk unless we infer supersolar abundances, an unusually large covering factor of reflecting material, or the presence of a high-energy cutoff in the incident spectrum between ~ 60 and ~ 200 keV.

We wish to thank Keith Jahoda for invaluable help with implementing and understanding the PCA calibration. We also thank the members of the *RXTE* Guest Observer Facility for their help with the data extraction. This research was supported by a NASA Long Term Space Astrophysics Grant.

REFERENCES

- Edwards, A. W. F. 1972, *Likelihood* (Cambridge: Cambridge University Press)
- Fabian, A. C., Rees, M. J., Stella, L., & White, N. E. 1989, *MNRAS*, 238, 729
- George, I. M. & Fabian, A. C. 1991, *MNRAS*, 249, 352
- Glasser, C. A., Odell, C. E., & Seufert, S. E. 1994, *IEEE Trans. Nucl. Sci.*, 41, 4
- Gondek, D. et al. 1996, *MNRAS*, 282, 646
- Guilbert, P. W. & Rees, M. J. 1988, *MNRAS*, 233, 475
- Laor, A. 1991, *ApJ*, 376, 90
- Lightman, A. P. & White, T. R. 1988, *ApJ*, 335, 57
- Magdziarz, P. & Zdziarski, A. A. 1995, *MNRAS*, 273, 837
- Nandra, K. & Pounds, K. A. 1994, *MNRAS*, 268, 405

- Nandra, K., George, I. M., Mushotzky, R. F., Turner, T. J., & Yaqoob, T. 1997, *ApJ*, 477, 602
- Pounds, K. A., Nandra, K., Stewart, G. C., George, I. M., & Fabian, A. C. 1990, *Nature*, 344, 132
- Smith, D. A. & Done C. 1996, *MNRAS*, 280, 355
- Tennant, A. F. 1983, Ph.D. Thesis, NASA Technical Memorandum #85101
- Turner, T. J., George, I. M., Nandra, K., & Mushotzky, R. F. 1997, *ApJ*, in press (T97)
- Veron, P. Lindblad, P. O., Zuiderwijk, E. J., Veron, M. P., & Adam, G. 1980, *AA*, 87, 245
- Weaver, K. A., Yaqoob, T., Mushotzky, R. F., Nousek, J., Hayashi, I., & Koyama, K. 1997, *ApJ*, 474, 675 (W97)
- Zdziarski, A. A., Johnson, W. N., & Magdziarz, P. 1996, *MNRAS*, 283, 193

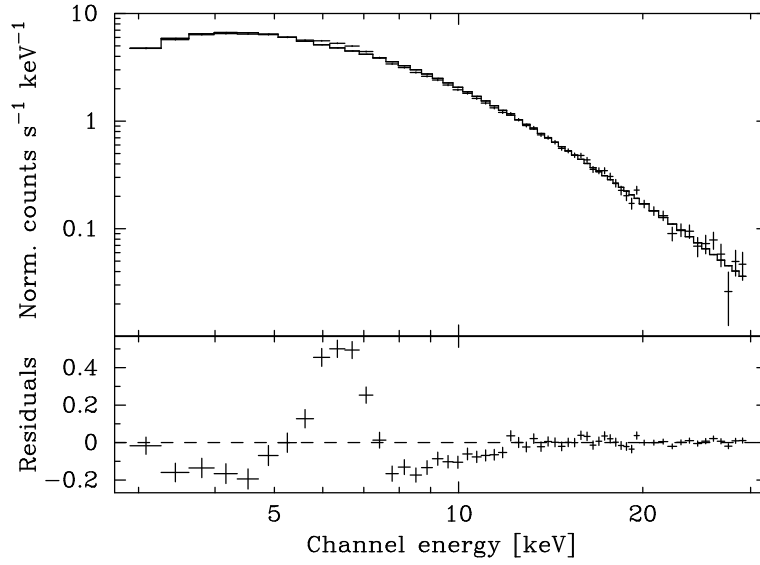


Fig. 1.— Data from the *RXTE* PCA and a model that consists of an absorbed power law (fit 1, Table 1) folded through the instrumental response. The residuals are plotted in the bottom panel.

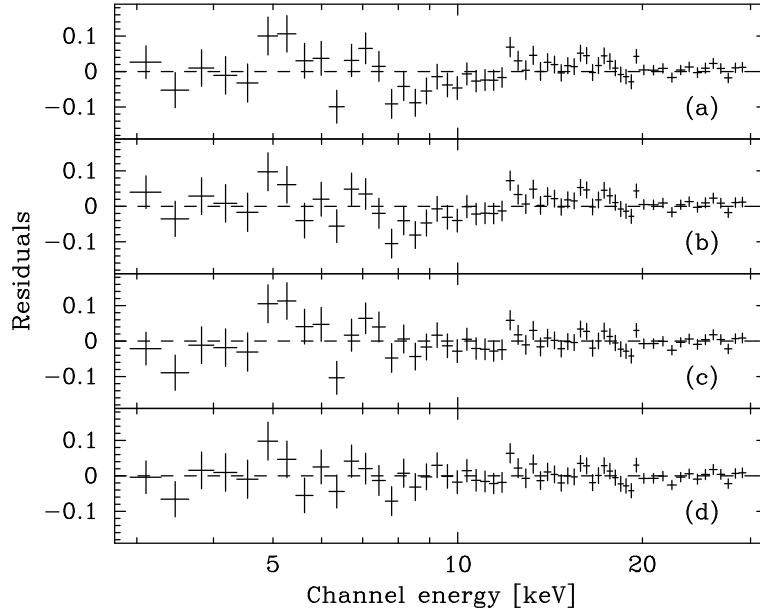


Fig. 2.— Residuals for fits listed in Table 1 for models that consist of (a) an absorbed power law and a narrow Fe $K\alpha$ line (fit 2), (b) an absorbed power law and a broad Fe $K\alpha$ line (fit 3), (c) an absorbed power law, Compton reflection, and a narrow Fe $K\alpha$ line (fit 4), and (d) an absorbed power law, Compton reflection, and a broad Fe $K\alpha$ line (fit 7). All of these fits are for the case with $E_c = 500$ keV and response matrix M8.

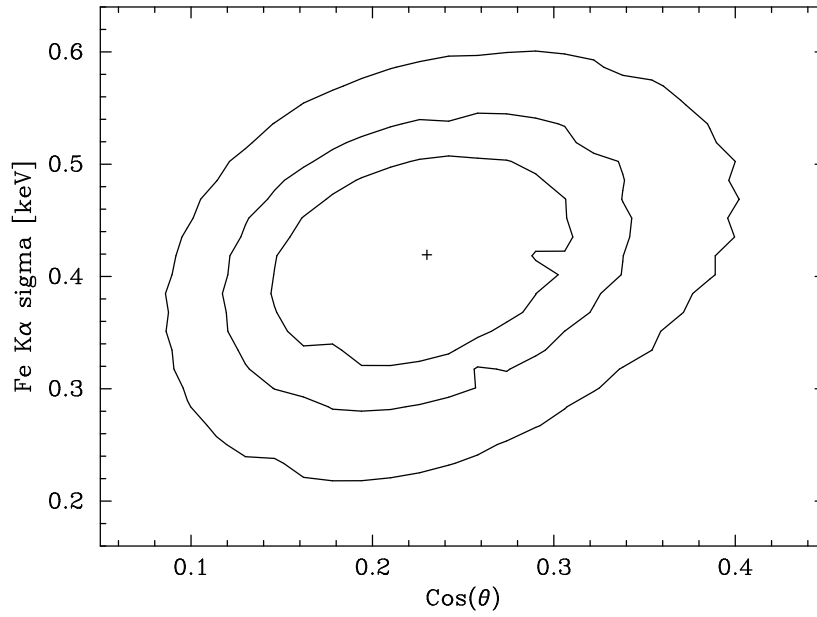


Fig. 3.— Confidence contours for the Fe K α line width vs. cosine of the disk inclination angle derived from the Compton reflection hump for $c_f = 0.5$ ($R=1.0$) and a primary power-law spectrum with $E_c = 200$ keV. (fit 7, Table 1).

TABLE 1
RXTE SPECTRAL FITTING RESULTS^a

(1)	(2)	(3)	(4)	(5)	(6)	(7)	(8)	(9)	(10)	(11)	(12)	(13)	(14)	(15)	(16)
Fit	Γ	A [10 ⁻²]	Fe K α Energy [keV]	W _{Kα} [eV]	Fe K α σ [keV]	i [$^\circ$]	R	ν	$\frac{\chi^2}{\nu}$ (M8)	$\frac{\chi^2}{\nu}$ (M85)	(x,y)	F _(x,y) ^{M8}	F _(x,y) ^{M85}	P _(x,y) ^{M8}	P _(x,y) ^{M85}
1	1.74±0.05	2.9±0.1	57	9.84	9.63
2	1.74±0.05	2.8±0.1	6.34±0.05	200±15	0.2(f)	55	1.55	1.49
3	1.74±0.05	2.8±0.1	6.31±0.07	223 ⁺²⁴ ₋₂₂	0.36 ^{+0.12} _{-0.14}	54	1.44	1.48	(2,3)	4.86	1.35	0.03	0.24
4	1.81±0.06	3.0±0.1	6.36±0.07	198 ⁺¹⁴ ₋₁₃ 189±15 172±15	0.2(f)	83 ⁺⁴ ₋₆ 77 ⁺⁶ ₋₉ 64 ⁺⁹ ₋₁₁	1.0(f)	54	1.18	1.09
5	1.80±0.06	3.0±0.2	6.31 ^{+0.09} _{-0.10}	232 ⁺²⁵ ₋₂₃ 226 ⁺²¹ 205 ⁺¹⁵ ₋₁₈	0.43±0.15	50(f)	0.36 ^{+0.24} _{-0.22} 0.45±0.23 0.80 ^{+0.24} _{-0.25}	53	1.02	1.04	(4,5)	9.80	3.85	0.002	0.05
6	1.84±0.06	3.1±0.2	6.32 ^{+0.09} _{-0.10}	229 ⁺²⁴ ₋₂₃ 213 ⁺¹⁷ 185 ⁺¹⁶ ₋₁₈	0.44 ^{+0.14} _{-0.15}	87(f)	2.9 ^{+2.0} _{-1.9} 3.4 ^{+2.6} 5.9 ^{+3.3} _{-1.7}	53	0.96	0.96	(4,6)	13.54	8.33	<0.001	0.005
7	1.81±0.05	3.1±0.2	6.31 ^{+0.09} _{-0.11}	230 ⁺²⁵ ₋₂₂ 223±17 200 ⁺¹⁷ ₋₁₆	0.43±0.15	81 ⁺⁶ ₋₇ 75 ⁺⁶ 63 ⁺¹⁰ ₋₁₃	1.0(f)	53	0.98	0.98	(4,7)	12.24	7.14	<0.001	0.008

¹Number assigned to the fit for reference in the text. The models for each are as follows: (1) power law, (2) power law plus a narrow Gaussian, (3) power law plus a broad Gaussian, (4) power law plus reflection plus a narrow Gaussian, and (5, 6, and 7) power law plus reflection plus a broad Gaussian.

²Photon index of primary power law spectrum. Errors include 1.5% systematic errors.

³Power-law normalization in units of [photons keV⁻¹ cm⁻² s⁻¹] at 1 keV. Errors include 1.5% systematic errors.

⁴Energy of the Fe K α line. Energies are corrected for redshift.

⁵Equivalent Width of the Fe K α line. The three values listed for fits 4 to 7 are for $E_c = 500, 200,$ and 60 keV, respectively.

⁶Physical width of the Fe K α line.

⁷The inclination angle of the disk normal to our line of sight; $i=0$ is face-on. The three values listed for fits 4 and 7 are for $E_c = 500, 200,$ and 60 keV, respectively.

⁸Relative normalization of reflection with respect to the primary power law. For a flat disk geometry with $\Omega/2\pi = 1$ and an isotropic source, $R = 1$. The three values listed for fits 5 and 6 are for $E_c = 500, 200,$ and 60 keV, respectively.

⁹Number of degrees of freedom.

¹⁰Reduced χ^2 for response matrix M8.

¹¹Reduced χ^2 for response matrix M85.

¹²The values of x and y are the numbers assigned to the fits in column 1.

¹³F-statistic for response M8 comparing fit x with fit y.

¹⁴F-statistic for response M85 comparing fit x with fit y.

¹⁵Probability of exceeding F for response M8.

¹⁶Probability of exceeding F for response M85.

^aThe letter f denotes a fixed parameter. Errors for normalization, Fe K Energy, and W_{K α} are 90% confidence for one interesting parameter ($\chi^2+2.7$). Other errors are 90% confidence for two (fits 1 – 3) or three (fits 4 – 7) interesting parameters.